Available online at www.sciencedirect.com
ScienceDirect
Journal of the European Ceramic Society 31 (2011) 705–714
www.elsevier.com/locate/jeurceramsoc

Dynamic corrosion of Al_2O_3–ZrO_2–SiO_2 and Cr_2O_3-containing refractories by molten frits. Part II: Microstructural study

P. Pena [a,*], E. Criado [a], J.J. Bakali [b,c], C. Baudín [a]

[a] *Instituto de Cerámica y Vidrio, CSIC, Kelsen 5, 28049 Madrid, Spain*
[b] *Esmaltes S.A. Ctra. Castellón km 22,5, 12110 Alcora, Castellón, Spain*

Received 4 November 2010; received in revised form 19 November 2010; accepted 22 November 2010
Available online 28 December 2010

Abstract

In this work results on dynamic corrosion studies of fused cast Al_2O_3–SiO_2–ZrO_2 and isostatically pressed and sintered Cr_2O_3-based refractories by two crystalline (transparent) frits are described. Experiments have been performed using the "Merry Go Round" test at ≅1500 °C.

Microstructural and mineralogical analyses of selected areas from the corroded regions of the studied refractories were performed by reflected light optical microscopy and scanning electron microscopy with analysis by X-ray dispersive energy.

Significant differences between the corrosion mechanisms acting in the two types of materials were found. In the fused cast Al_2O_3–SiO_2–ZrO_2 specimens corrosion took place by the dissolution of alumina and zirconia in the frit and in the glass formed by the reaction between the frit and the refractory. In the Cr_2O_3-based materials the corrosion process was controlled by the capillar penetration of the molten frit through the open pores. The reaction between the ZnO from the frits and Cr_2O_3 led to the formation of spinel ($ZnCr_2O_4$), a high-melting point bonding phase that retarded the frit penetration. Results are discussed using the relevant phase equilibrium diagrams.

Keywords: Refractories; Corrosion; Al_2O_3; Cr_2O_3; ZrO_2; Microstructure-final

1. Introduction

As discussed in Part I of this work,[1] the production of frits is a main factor for the development of the tile industry. Frits are constituted by a relatively large number of components whose proportions are selected to reach the required characteristics. As some of the components such as K_2O, Na_2O, ZnO or B_2O_3 are highly corrosive, the critical factor in frit production is the life of the furnace. In spite of this, very little work has been done to improve refractory selection and most fabricants accept the high consumption of refractories as intrinsic for frit production. However, the new economical situation together with environmental issues demands changes in the way in which refractories are used in the frit industry.

The selection of the most adequate materials as a function of the chemical composition of the considered frit and the fabrication procedure requires the understanding of the corrosion process. In this work, corrosion by frits of the refractories currently used in glass and frit furnaces, Al_2O_3–ZrO_2–SiO_2 fused cast refractories (hereafter referred as AZS) and Cr_2O_3-based materials, is analysed. The microstructure of fused cast AZS blocks after manufacturing is well known and even described in the catalogues of these products. However the mineralogical changes after being used in glass melting furnaces have scarcely been reported.[2–5] Moreover, as far as the present authors know, such analysis has never been reported for the corrosion of any kind of refractory by frits.

Two refractories of each quality, AZS and Cr_2O_3-based, and two different crystalline frits, with characteristic compositions for low and high temperature tile enamelling (LTF, HTF) have been considered to determine the basic mechanisms as well as the influence of microstructural features on corrosion. The "Merry Go Round" test, currently used in the glass industry, has been chosen for corrosion to assure dynamic conditions. In Part I of the present work,[1] macroscopic results were analysed in the same way as they are in the glass industry. The microstructural analysis of the "as received" AZS electrofused

* Corresponding author.
E-mail address: ppena@icv.csic.es (P. Pena).
[c] Actual address: Parque Lidón, Torre 4, 8°B, 12003 Castellón, Spain.

0955-2219/$ – see front matter © 2010 Elsevier Ltd. All rights reserved.
doi:10.1016/j.jeurceramsoc.2010.11.024

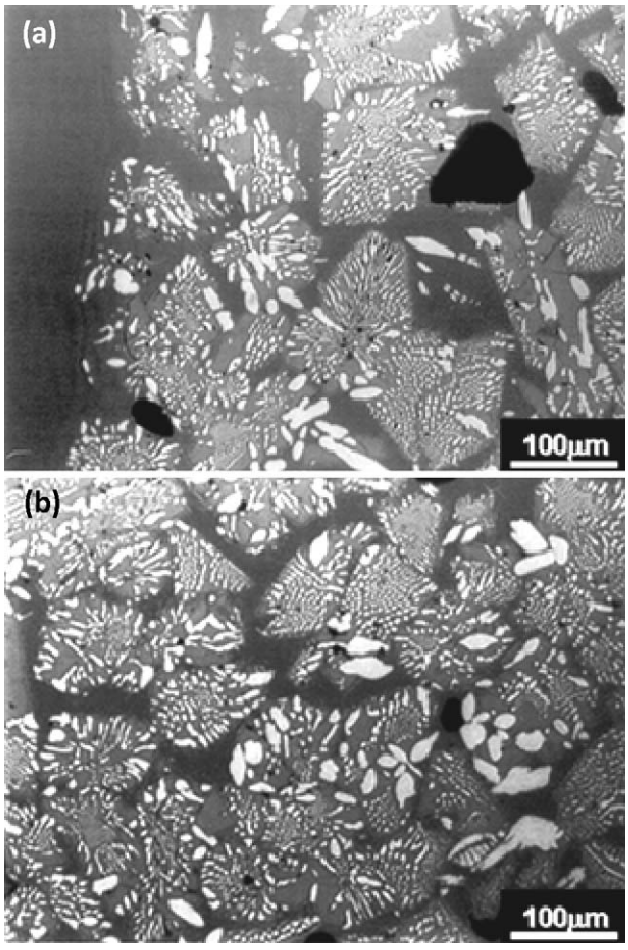

Fig. 1. Characteristic features of the reaction between the electrofused AZS refractory with 36 wt.% of ZrO_2 (AZS1681) and the high temperature frit (HTF). Reflected light optical microscopy micrograph of a polished cross section of a finger after 24 h testing using the "Merry Go Round" dynamic corrosion test at ≅1500 °C. The eutectic structure of the refractory formed by small zirconia (white) particles surrounded by alumina (grey) is observed. Large primary zirconia grains are also present. The phase surrounding the eutectic colonies (dark grey) is glass. (a) Interface between the frit (dark grey, left) and the refractory. (b) Microstructure at a distance of 4500 μm of the interface. The original microstructure of the material is observed.

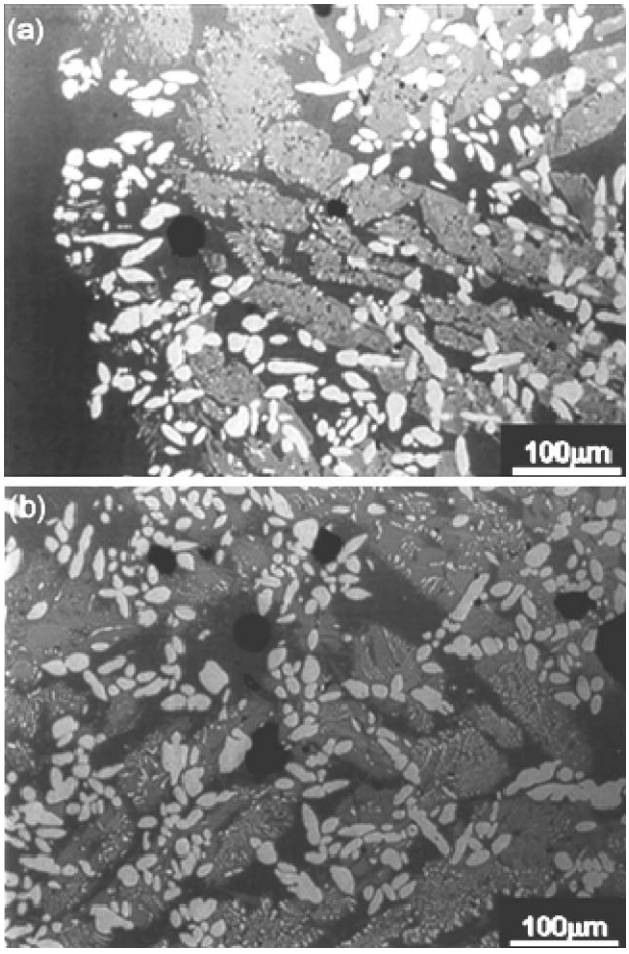

Fig. 2. Characteristic features of the reaction between the electrofused AZS refractory with 40 wt.% of ZrO_2 (AZS1711) and the high temperature frit (HTF). Reflected light optical microscopy micrograph of a polished cross section of a finger after 24 h testing using the "Merry Go Round" dynamic corrosion test at ≅1500 °C. The eutectic structure of the refractory formed by small zirconia (white) particles surrounded by alumina (grey) is observed. Large primary zirconia grains are also present. The phase surrounding the eutectic colonies (dark grey) is glass. (a) Interface between the frit (dark grey, left) and the refractory. (b) Microstructure at a distance of 3000 μm of the interface. The original microstructure of the material is observed.

materials together with the characteristics of the frits and the macroscopic results indicated that the extent of corrosion experienced by the AZS materials could be attributed to the progression of reactions at the contact zone between the external surface of the refractory and the frit. The Cr_2O_3-based specimens experienced volumetric increases during the test, thus, the meaning of the results of the macroscopic analysis was unclear. In this second part, the microstructural study of corroded samples is presented, and the corrosion mechanisms are described and discussed.

2. Experimental

The chemical and mineralogical composition as well as the microstructural characteristics of the four refractory materials studied and the chemical composition and viscosity at the testing temperature of the two frits were reported in Part I of this work.[1]

The fused cast AZS refractories were constituted by m-ZrO_2 (baddeleyite) and α-Al_2O_3 (corundum) as major constituents, contained about 12 wt.% of a Na-aluminosilicate glass and presented very low levels of open porosity (≅1.5%). The main difference between the materials was the ZrO_2 content (36 wt.% and 40 wt.% of ZrO_2, for materials AZS1681 and AZS1711, respectively).

Cr_2O_3 was the major constituent of both Cr_2O_3-containing materials (84.9 and 95.4 wt.% for materials ZC-85 and CR-95WB, respectively) which had high values of open porosity (≅16 and 17% for materials CR-95WB and ZC-85, respectively). In the material with the highest amount of Cr_2O_3, the aggregates were bonded by fine Cr_2O_3 grains whereas in the material with the lowest amount of Cr_2O_3, fine ZrO_2 particles and residual glass were found bonding the fine Cr_2O_3 in the matrix. In agreement with the residual glass observed, this latter material contained a much higher amount of fluxing impurities

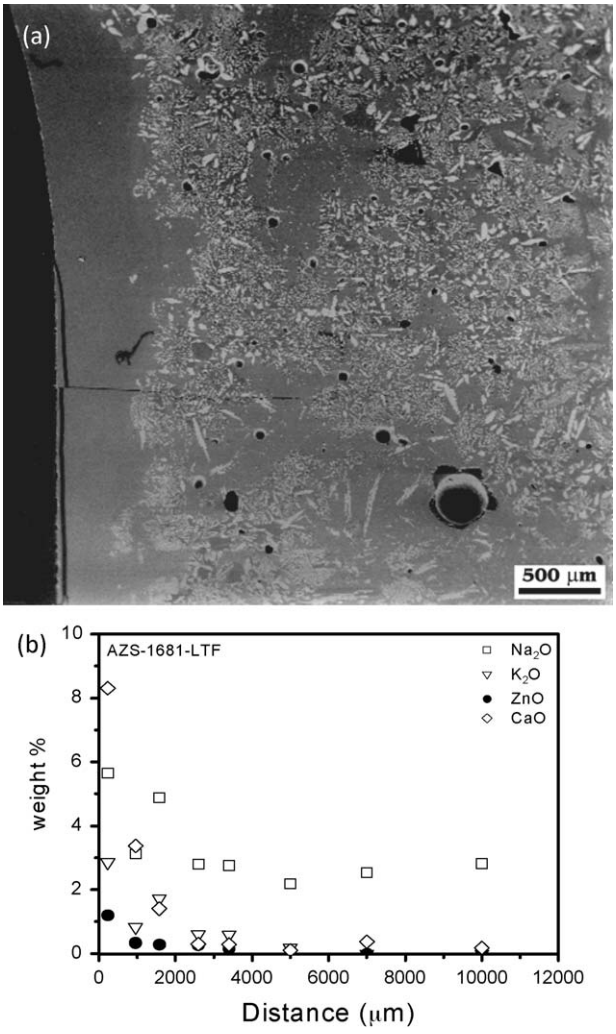

Fig. 3. Characteristic features of the reaction between the electrofused AZS refractory with 36 wt.% of ZrO_2 (AZS1681) and the low temperature frit (LTF). (a) Low magnification scanning electron microscopy micrograph of a polished cross section of a finger after 24 h testing using the "Merry Go Round" dynamic corrosion test at ≅1500 °C. The reaction layer between the frit (left, grey) and the refractory is shown. The present phases are identified in Fig. 5. (b) Presence of the constituents of the frit as a function of the distance from the frit–refractory interface. Na_2O was also present in the original refractory. X-ray dispersive energies analyses (SEM-EDS).

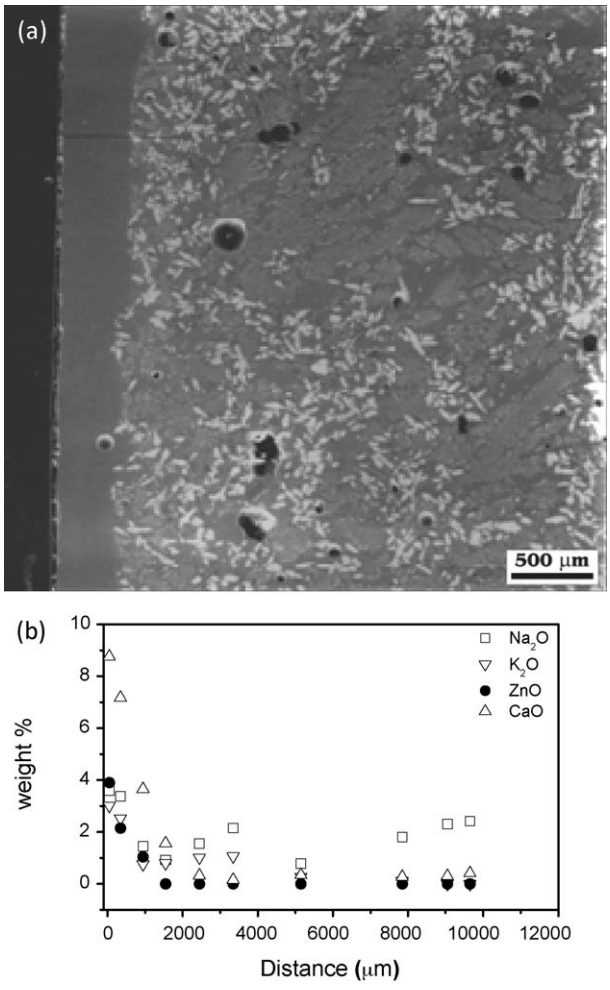

Fig. 4. Characteristic features of the reaction between the electrofused AZS refractory with 40 wt.% of ZrO_2 (AZS1711) and the low temperature frit (LTF). (a) Low magnification scanning electron microscopy micrograph of a polished cross section of a finger after 24 h testing using the "Merry Go Round" dynamic corrosion test at ≅1500 °C. The reaction layer between the frit (left, grey) and the refractory is shown. The present phases are identified in Fig. 6. (b) Presence of the constituents of the frit as a function of the distance from the frit–refractory interface. Na_2O was also present in the original refractory. X-ray dispersive energies analyses (SEM-EDS).

(Al_2O_3, alkalines and alkaline earths; ≈4 wt.%) than material CR-95WB (≈0.3 wt.%). Both materials contained the typical impurities of Cr_2O_3 (TiO_2 and SiO_2).

Main differences between the frits were the amounts of fluxing agents, B_2O_3, K_2O and Na_2O, that were the highest in the LTF, and the amount of ZnO, which was the highest in the HTF. Both frits were completely melted at the testing temperature (≅1500 °C) with viscosities $\log \eta = 2.1$ and 2.2 (η in Pa s) for the LTF and HTF, respectively.

The characteristics of the corrosion test are described in Part I.[1] Refractory specimens in the shape of cylinders of 120 mm length and 20 mm diameter ("fingers") were tested immersed in the molten frit (≅1500 °C) in a rotary furnace for 24 h.

For the microstructural characterization after testing, cross sections of the cylinders (i.e., sections perpendicular to the frit–refractory interfaces) were diamond cut and mounted using a cold setting resin. Standard ceramographic grinding and polishing techniques were then carried out on these cross sections.

The first microstructural analyses and phase identification were done by reflected-light optical microscopy (RLOM, Model HP 1, Carl Zeiss, Oberköchen and Jena Gmb, Germany). Then further analyses were done using scanning electron microscopy with energy dispersive X-ray spectroscopy (SEM-EDS, Model DSM 950, Karl Zeiss, Thornwood, NY; series, Tracor Northern, Middleton, WI). Microchemical analyses were carried out by SEM-EDS to determine the composition of the observed phases and to establish the diffusion profile of different elements. Counting times were 60 s. Semiquantitative analyses were done using the ZAF (Atomic number, Absorption, Fluorescence) correction performed by the software provided with the equipment.

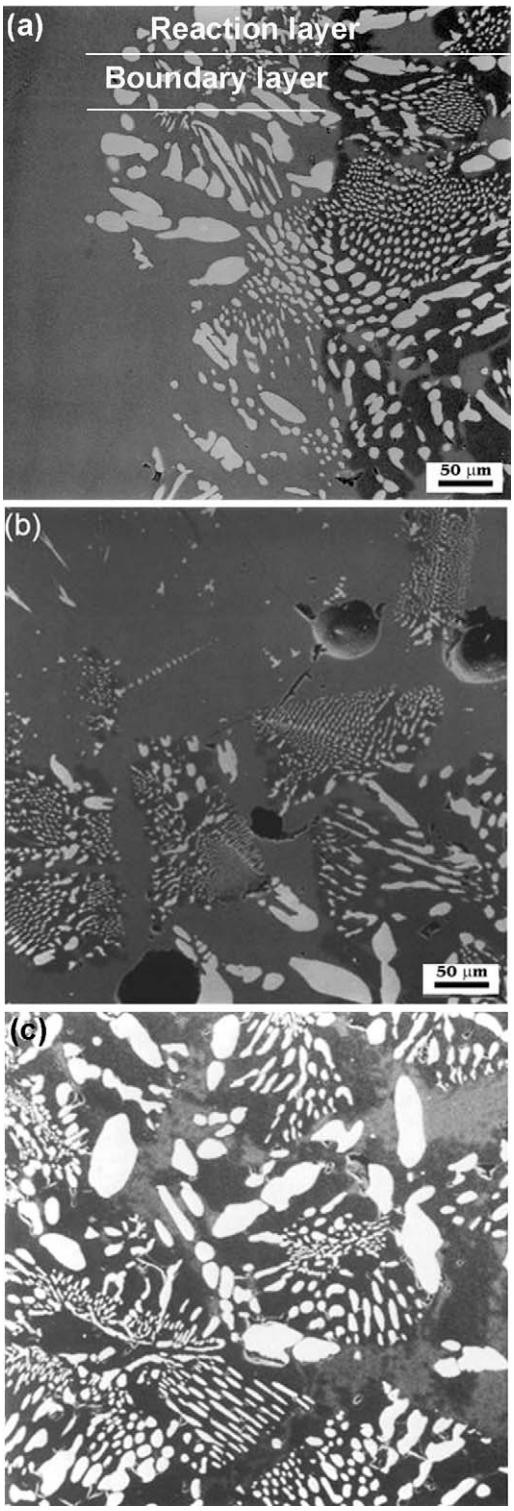

Fig. 5. Characteristic features of the reaction between the electrofused AZS refractory with 36 wt.% of ZrO_2 (AZS1681) and the low temperature frit (LTF). Scanning electron microscopy micrograph of a polished cross section of a finger after 24 h testing using the "Merry Go Round" dynamic corrosion test at ≅1500 °C. The white particles are zirconia, the dark grey phase is alumina and the light grey phase is glass. (a) Interface between the frit (left) and the refractory. The boundary layer of zirconia particles and glass formed in the reaction layer at the frit–refractory interface is observed. (b) Reaction layer at a distance of 1000 μm of the interface. (c) Reaction layer at a distance of 2000 μm of the interface.

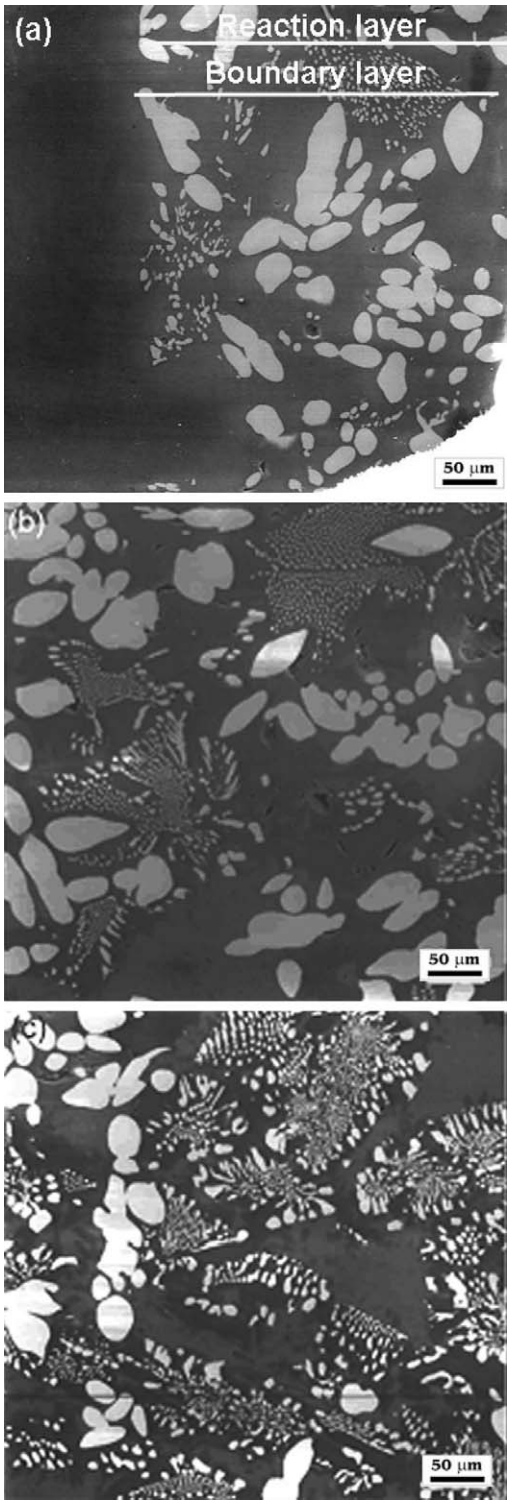

Fig. 6. Characteristic features of the reaction between the electrofused AZS refractory with 40 wt.% of ZrO_2 (AZS1711) and the low temperature frit (LTF). Scanning electron microscopy micrograph of a polished cross section of a finger after 24 h testing using the "Merry Go Round" dynamic corrosion test at ≅1500 °C. The white particles are zirconia, the dark grey phase is alumina and the light grey phase is glass. (a) Interface between the frit (left) and the refractory. The boundary layer of zirconia particles and glass formed in the reaction layer at the frit–refractory interface is observed. (b) Reaction layer at a distance of 1000 μm of the interface. (c) Reaction layer at a distance of 2000 μm of the interface.

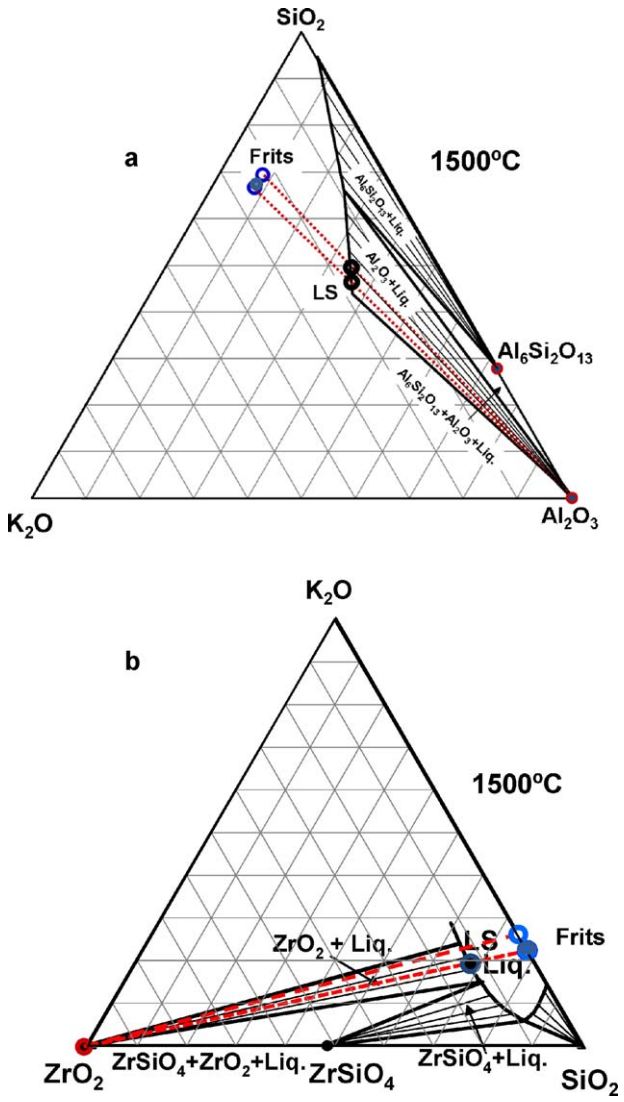

Fig. 7. Isothermal sections at 1500 °C of the regions of the ternary equilibrium phase diagrams used for the discussion of the corrosion process of the AZS refractories by the HTL (hollow circle) and the LTF (solid circle). The simplified compositions of both frits (Table 1) and the connecting lines between these compositions and the refractory crystalline component that is being dissolved in the frit are plotted. LS is the solubility limit of the component in the liquid and corresponds to the composition of the liquid in equilibrium with the component. (a) System Al_2O_3–SiO_2–K_2O used to discuss the dissolution of the eutectic Al_2O_3. (b) System ZrO_2–SiO_2–K_2O used to discuss the dissolution of the eutectic and the primary ZrO_2.

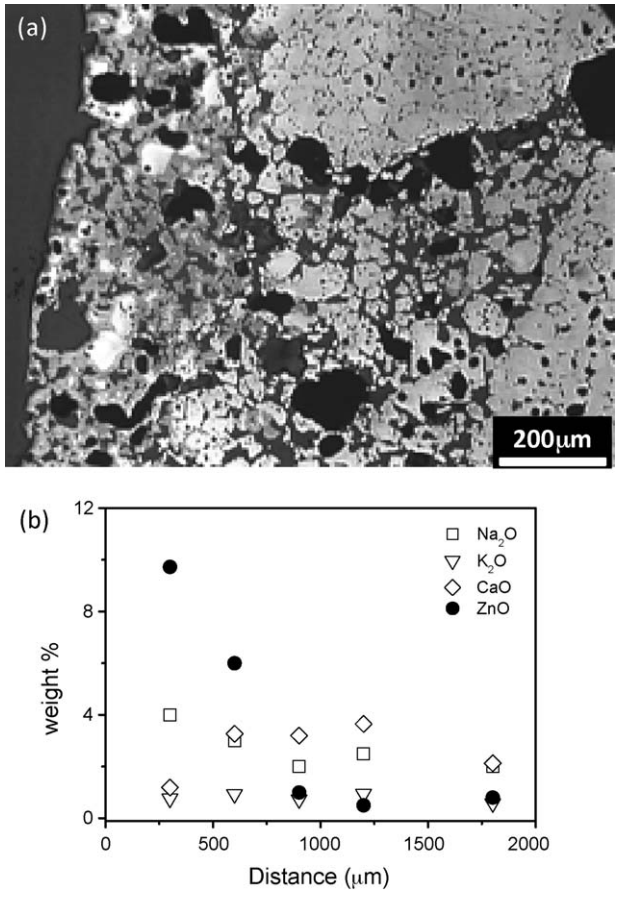

Fig. 8. Characteristic features of the reaction between the isopressed Cr_2O_3-refractory with 96 wt.% of Cr_2O_3 (CR-95WB) and the high temperature frit (HTF). Results obtained on a polished cross section of a finger after 24 h testing using the "Merry Go Round" dynamic corrosion test at ≅1500 °C. The grey grains are Cr_2O_3, the major component of the refractory. Pores are round and black. (a) Interface between the frit (left) and the refractory. The white grains were identified as $ZnCr_2O_4$ by analysis by X-ray dispersive energies analysis (SEM-EDS). Reflected light optical microscopy micrograph. (b) Presence of the constituents of the frit as a function of the distance from the frit–refractory interface. Na_2O was also present in the original refractory. The maximum penetration distances were ≈200 μm for ZnO and ≈2000 for the other frit constituents. X-ray energies dispersive analyses.

Under the experimental conditions used in this work it was not possible to obtain the X-ray energy signal corresponding to B.

3. Results and discussion

Corrosion of a refractory by a liquid is an irreversible process occurring in a heterogeneous open system that implies chemical exchanges. Such exchanges would take place fundamentally through the vulnerable portion of the refractory, by diffusion of the liquid through the grain boundaries and the residual glass and by capillar infiltration through the open pores. Corrosion will be enhanced in the case of low viscosity and surface tension liquids such as the molten frits used for the corrosion studies.

The differences between the chemical composition and the microstructural features of the studied materials led to different corrosion processes, as discussed below.

3.1. Fused cast Al_2O_3–SiO_2–ZrO_2 refractories

The original microstructures of the fused cast AZS refractories were made of interlocking alumina–zirconia eutectic polycrystals and large primary zirconia grains embedded in glass.[1] Such microstructures presented similar low levels of open porosity (≈1.5 wt.%), the main difference between them being the ZrO_2 content.

The characteristic features of the corrosion process of AZS refractories by the frits are shown in Figs. 1–6. Similar microstructural modifications were found for both frits the only

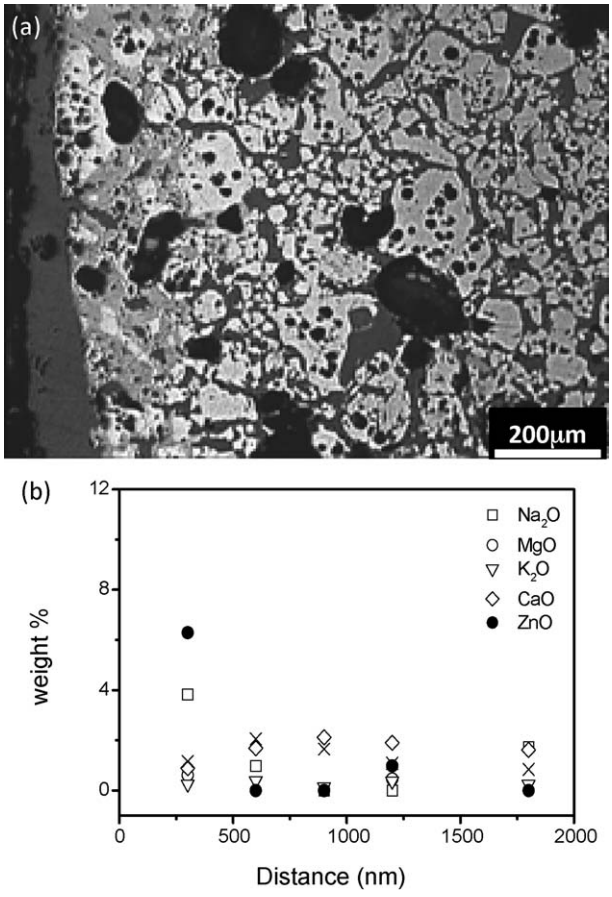

Fig. 9. Characteristic features of the reaction between the isopressed Cr_2O_3-refractory with 84 wt.% of Cr_2O_3 (ZC-85) and the high temperature frit (HTF). Results obtained on a polished cross section of a finger after 24 h testing using the "Merry Go Round" dynamic corrosion test at ≅1500 °C. The grey grains are Cr_2O_3, the major component of the refractory. Pores are round and black. (a) Interface between the frit (left) and the refractory. The white grains were identified as $ZnCr_2O_4$ by analysis by X-ray dispersive energies (SEM-EDS). Reflected light optical microscopy micrographs. (b) Presence of the constituents of the frit as a function of the distance from the frit–refractory interface. Na_2O was also present in the original refractory. The maximum penetration distances were ≈1000 for all the frit constituents. X-ray energy dispersive analyses (SEM-EDS).

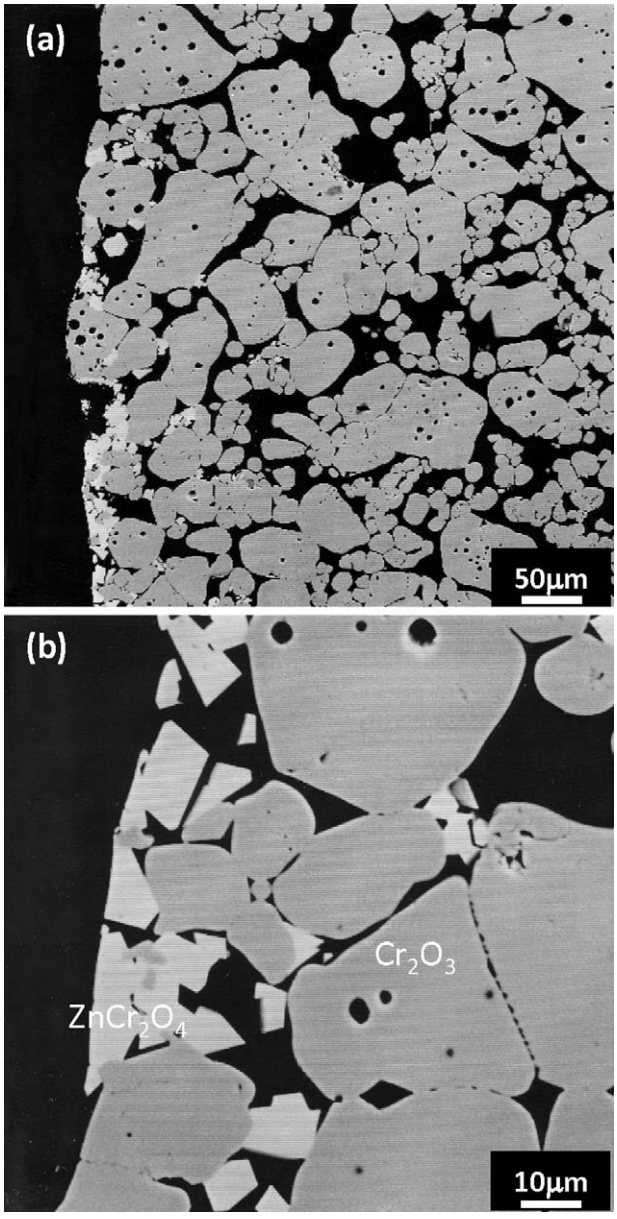

Fig. 10. Characteristic features of the reaction between the isopressed Cr_2O_3-refractory with 96 wt.% of Cr_2O_3 (CR-95WB) and the low temperature frit (LTF). Scanning electron microscopy micrographs of a polished and chemically etched (HF 10 vol.%–15 s) cross section of a finger after 24 h testing using the "Merry Go Round" dynamic corrosion test at ≅1500 °C. (a) Low magnification. A reaction layer (width < 50 μm) is observed at the interface between the frit (left) and the refractory. (b) Detail of the reaction layer formed by white particles between some of the Cr_2O_3 grains. The white particles were identified as $ZnCr_2O_4$ by X-ray dispersive energies analysis (SEM-EDS).

difference being a slightly larger reaction layer in the specimens tested using the low temperature frit (LTF) than in the ones tested using the high temperature frit (HTF). The penetration depths of the frit constituents and the widths of the corroded layers differentiated by RLOM and SEM were always smaller in the specimens of the refractory containing the highest amount of ZrO_2 (40 wt.%, AZS1711) than in the AZS1681 ones. Neither the formation of new crystalline phases nor recrystallization of phases were detected in any of the interfaces studied.

The low magnification micrographs of Figs. 1 and 2 show that, for specimens tested using the HTF, the original microstructures were found at distances from the frit–refractory interface of about 4500 and 3000 μm for the materials containing 36 wt.% and 40 wt.% of ZrO_2, respectively. For both materials, corroded layers of highly modified microstructure were observed close to the frit–refractory interfaces (Figs. 1a and 2a). These reaction layers were characterised by the absence of Al_2O_3 surrounding the eutectic ZrO_2 particles.

The chemical analyses of the reaction layers (Figs. 3 and 4) revealed the presence of the constituents of the frits. As shown in Figs. 3b and 4b for specimens tested using the LTF, Na_2O, K_2O and CaO penetrated through the whole reaction layers (distances about 4500 and 3000 μm for the materials containing 36 wt.% and 40 wt.% of ZrO_2, respectively) whereas the penetration of ZnO was limited to the most external regions of the reaction

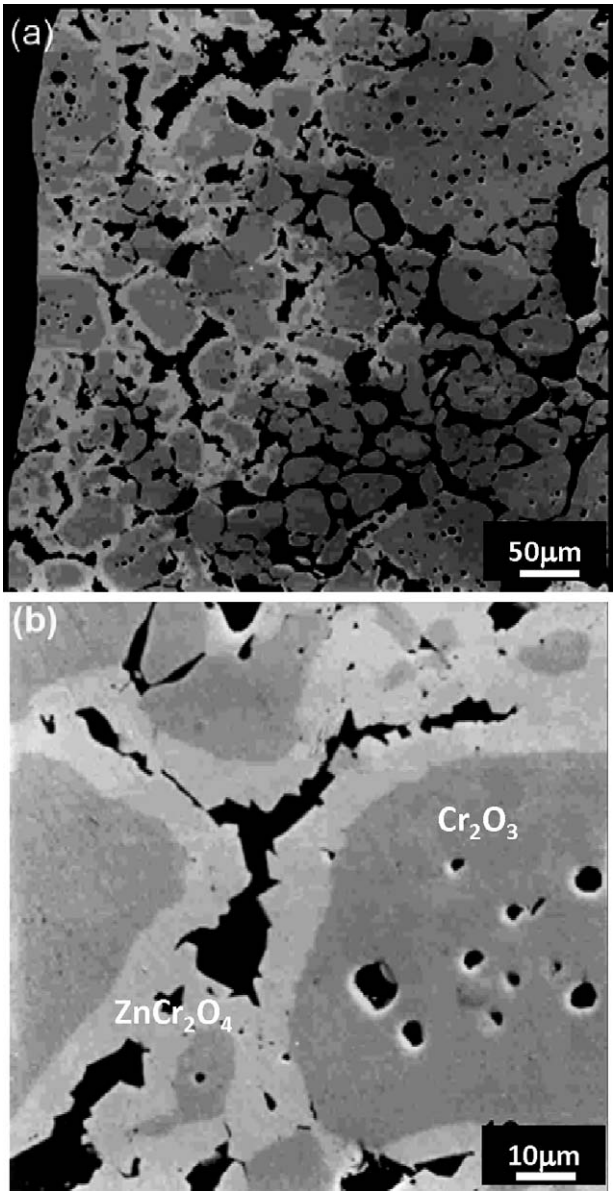

Fig. 11. Characteristic features of the reaction between the isopressed Cr_2O_3-refractory with 96 wt.% of Cr_2O_3 (CR-95WB) and the low temperature frit (LTF). Scanning electron microscopy micrographs of a polished and chemically etched (HF 10 vol.%–15 s) cross section of a finger after 24 h testing using the "Merry Go Round" dynamic corrosion test at ≅1500 °C. (a) Low magnification. A reaction layer (width ≈ 200 μm) is observed at the interface between the frit (left) and the refractory. (b) Detail of the reaction layer formed by white particles forming a continuous phase that surrounds the Cr_2O_3 grains. The white particles were identified as $ZnCr_2O_4$ by X-ray dispersive energies analysis (SEM-EDS).

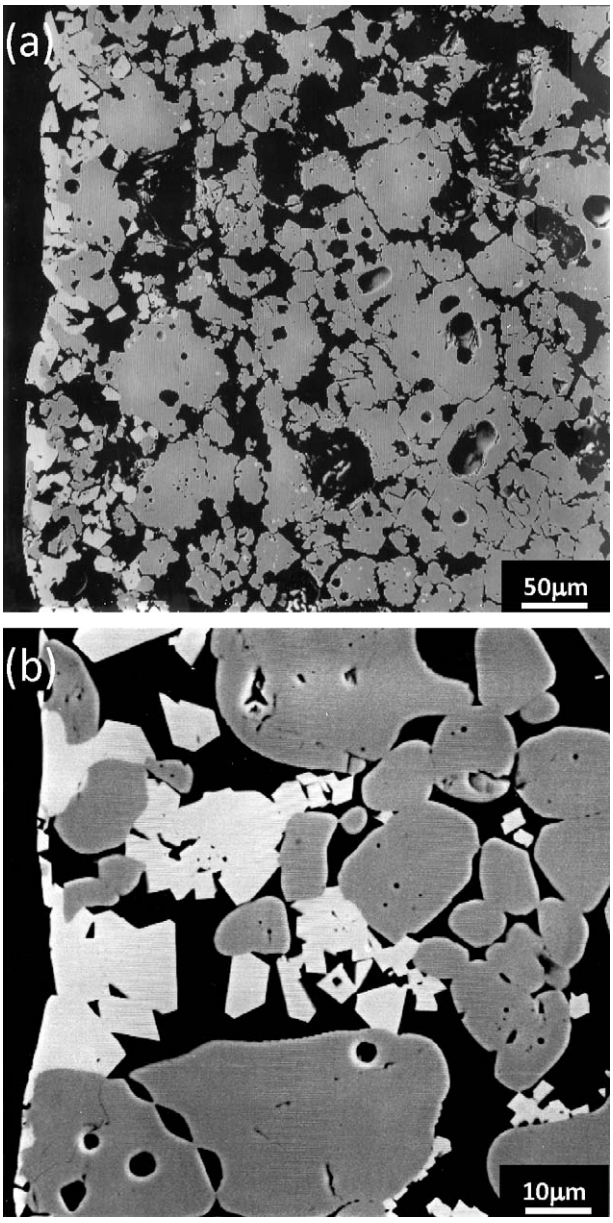

Fig. 12. Characteristic features of the reaction between the isopressed Cr_2O_3-refractory with 84 wt.% of Cr_2O_3 (ZC-85) and the low temperature frit (LTF). Scanning electron microscopy micrographs of a polished and chemically etched (HF 10 vol.%–15 s) cross section of a finger after 24 h testing using the "Merry Go Round" dynamic corrosion test at ≅1500 °C. (a) Low magnification. A reaction layer (width < 100 μm) is observed at the interface between the frit (left) and the refractory. (b) Detail of the reaction layer formed by white particles between some of the Cr_2O_3 grains. The white particles were identified as $ZnCr_2O_4$ by X-ray dispersive energies analysis (SEM-EDS).

layers (distances about 2000 and 1500 μm for the materials containing 36 wt.% and 40 wt.% of ZrO_2, respectively). Thus, the absence of ZnO did not arrest the corrosion process.

Details of the microstructures of the reaction layers are shown in Figs. 5 and 6. For both materials and both frits, boundary layers constituted by zirconia particles surrounded by a SiO_2-rich glass were found close to the frit–refractory interfaces (Figs. 5a and 6a). Most of these particles were large which indicated that they were the primary ZrO_2 ones. Those coming from the eutectic structure were also found forming groups of small particles. For specimens tested using the LTF, the widths of the boundary layers were about 300 and 250 μm for the materials containing 36 wt.% (Fig. 5a) and 40 wt.% of ZrO_2 (Fig. 6a), respectively. Large amounts of glass were also found deeper into the refractories, in the zones reached by the constituents of the frits (Figs. 5b,c and 6b,c). The amounts of glass decreased and the amounts of eutectic ZrO_2–Al_2O_3 colonies increased as the proportion of frit constituents decreased in both materials (Figs. 3b, 4b, 5b,c and 6b,c).

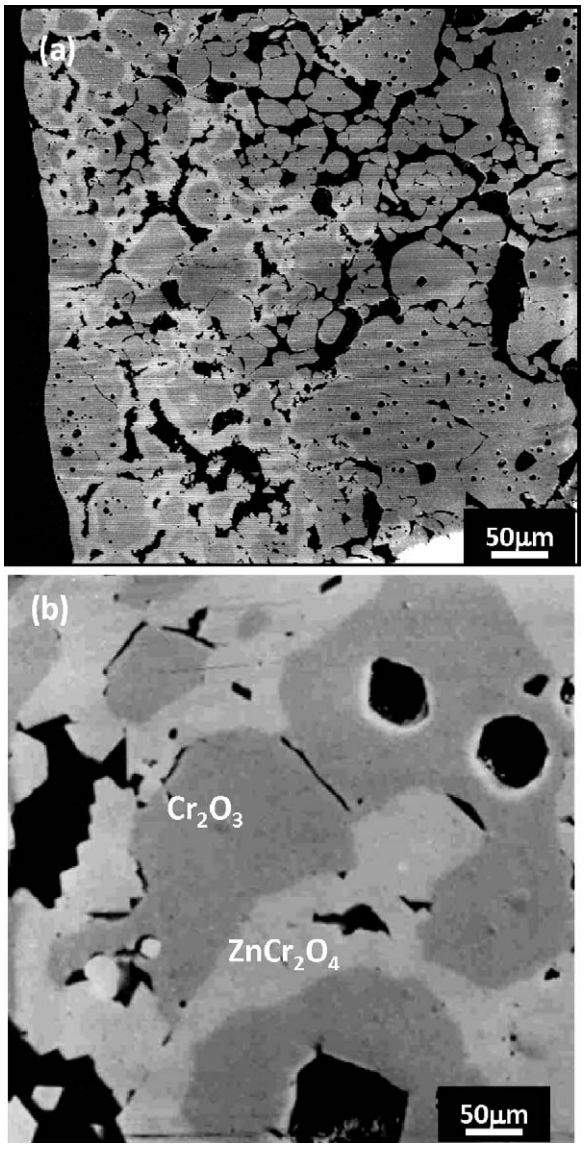

Fig. 13. Characteristic features of the reaction between the isopressed Cr_2O_3-refractory with 84 wt.% of Cr_2O_3 (ZC-85) and the high temperature frit (HTF). Scanning electron microscopy micrographs of a polished and chemically etched (HF 10 vol.%–15 s) cross section of a finger after 24 h testing using the "Merry Go Round" dynamic corrosion test at ≅1500 °C. (a) Low magnification. A reaction layer (width ≈ 500 μm) is observed at the interface between the frit (left) and the refractory. (b) Detail of the reaction layer formed by white particles forming a continuous phase that surrounds the Cr_2O_3 grains. The white particles were identified as $ZnCr_2O_4$ by X-ray dispersive energies analysis (SEM-EDS).

The microstructural features of the corrosion process summarized above demonstrate that in the fused cast AZS refractories corrosion at the frit–refractory interface started by the direct dissolution of the Al_2O_3 from the eutectic colonies in the fused frit. To a lesser extent, the small ZrO_2 particles from the eutectic colonies were also dissolved whereas the large primary ones were more resistant. Then corrosion advanced by diffusion of the frit constituents into the refractory and further dissolution of Al_2O_3 and ZrO_2 in the liquid formed by reaction between the frit and the refractory constituents.

The boundary layers were thicker in the specimens of the material containing the highest amount of ZrO_2 (AZS1711) which contained a higher amount of primary ZrO_2 than in the AZS1681 ones. The lack of new crystalline products demonstrates that the reaction of Al_2O_3 and ZrO_2 with the molten frits occurs by dissolution of the crystalline phases.

Differences between the corrosion levels of different AZS tested specimens were mainly dependent on the composition of the constituent material and not on that of the frit used for testing. The saturation limits for the solubility of the refractory constituents, Al_2O_3 and ZrO_2, in the frits would determine the dissolution process. The exact values of these limits are not available. Moreover, they cannot be determined from the analyses of the tested specimens, as is usually done in post-mortem analyses of AZS materials used in glass tanks, because the equilibrium has not been reached under the experimental conditions used. However, the differences between the dissolution behaviour of Al_2O_3 and ZrO_2 can be discussed using the phase equilibrium relationships in the involved systems, specifically Al_2O_3–SiO_2–ZnO,[6] Al_2O_3–SiO_2–alkali,[7] Al_2O_3–SiO_2–ZnO–alkali, ZrO_2–SiO_2–alkali,[8], ZrO_2–SiO_2–ZnO–alkali and Al_2O_3–SiO_2–ZrO_2–ZnO–alkali. As the complete information is not available, the discussion that follows has been performed using three component equilibrium relationships taking into account the glass structure theories of Zachariasen[9] and Dietzel.[10] According to these authors, SiO_2 and B_2O_3 are glass network formers while alkalies, alkaline earths and ZnO are network modifiers or fluxing elements; Al_2O_3 and ZrO_2 have intermediate character and will act as network formers when present in relatively high amounts.

As compared to ZnO, K_2O and Na_2O have a much stronger fluxing effect on Al_2O_3–SiO_2 mixtures[7]; liquidus temperatures as low as 985 °C and 1000 °C associated with significant quantities of liquid phase are expected. There are no data for the corresponding equilibrium relationships when ZnO–ZrO_2–SiO_2 mixtures are considered, however, it is reasonable to expect the same kind of relative effects. Therefore, the discussion of Al_2O_3 and ZrO_2 solubility in the frits can be done on the basis of Al_2O_3–SiO_2–alkali compositions and ZrO_2–SiO_2–alkali compositions, associating the total amounts of alkalines, alkaline earths and ZnO to the alkali amounts in the simplified frit compositions.

The amounts of K_2O present in both frits are higher than those of Na_2O. Moreover, the invariant point in the high SiO_2 region of the Al_2O_3–SiO_2–K_2O system is slightly lower (≈90 °C) than that for Al_2O_3–SiO_2–Na_2O. Therefore, the isothermal sections for the ternary systems Al_2O_3–SiO_2–K_2O and ZrO_2–SiO_2–K_2O at the working temperature, 1500 °C (Fig. 7) were chosen to analyze the solubility of the crystalline components of the refractories in the frits. In Table 1 the simplified chemical compositions of the frits to work in the ternary systems are shown. For the Al_2O_3–SiO_2–K_2O system, the simplified frit compositions have the three components. The total amount of network formers, SiO_2 and B_2O_3, was associated to the SiO_2 while the total amount of modifiers, alkalies, alkaline earths and ZnO, was taken as the total amount of K_2O. In this case, the ternary component is Al_2O_3 and the level of dissolution of eutectic Al_2O_3 from the AZS refractory will be lowered for increasing amounts of this ternary component in the frit. The simplified frit compositions

Table 1
Simplified compositions of the frits calculated from the major components considering the Al_2O_3–SiO_2–modifier and ZrO_2–SiO_2–modifier systems.

Frit	Approach to system	Composition (wt.%)		
		$SiO_2 + B_2O_3$	$Na_2O + K_2O + CaO + ZnO$	Al_2O_3
HTF	Al_2O_3–SiO_2–modifier	64.5	27.5	8.0
	ZrO_2–SiO_2–modifier	72.5	27.5	0
LTF	Al_2O_3–SiO_2–modifier	69.8	21.5	8.7
	ZrO_2–SiO_2–modifier	78.5	21.5	0

to work with the ZrO_2–SiO_2–K_2O system only have two components and the amount of Al_2O_3 in the original composition should be added to that of the glass forming constituents.

The calculated frit compositions are plotted in Fig. 7. Corrosion would proceed by dissolution of Al_2O_3 and ZrO_2, until the thermodynamic equilibrium between the resulting liquid and the crystalline phase is reached, hence, the corrosion paths may be represented by lines connecting the frit compositions with Al_2O_3 or ZrO_2.

When the Al_2O_3–SiO_2–K_2O system is considered (Fig. 7a), the liquid frits gradually wet and dissolve corundum grains moving the composition along the frit-Al_2O_3 connecting lines. The compositions of the frit–refractory interfaces change entering the stability field of α-Al_2O_3 + liquid until they reach the compositions of the liquids in equilibrium with alumina, thus, ending the corrosion process. The theoretical compositions of these liquids, called limits of saturation, are similar for both frits (LS point in Fig. 7a: 46–50 wt.% SiO_2, 35–36 wt.% Al_2O_3 and 15–18 wt.%, K_2O). For the interface liquid to reach equilibrium with Al_2O_3 in the refractory, its composition has to move to that of LS. Thus, taking into account the initial amount of Al_2O_3 in the frits (≈8 wt.%, Table 1) it would have to incorporate 27–28 wt.% of the refractory Al_2O_3.

In a similar way, considering the ZrO_2–SiO_2–K_2O isothermal section at 1500 °C, the theoretical compositions of the limit of saturation of ZrO_2 in the frits are in the ranges 63–67 wt.% SiO_2, 13 wt.% ZrO_2 and 20–23 wt.% K_2O.

The fact that the theoretical compositions of the limits of saturation of the refractory constituents, Al_2O_3 and ZrO_2 are similar for both frits justifies the observed similarity between the corrosion levels of the refractories by both frits.

The much higher theoretical amount of Al_2O_3 in the equilibrium saturated liquid (35–36 wt.%) as compared to that of ZrO_2 (≈13 wt.%) explains that ZrO_2 had lower solubility than Al_2O_3 in the frits used for the corrosion tests.

In these materials with extremely low open porosity, penetration of the frit into the bulk took place preferentially through the residual glass and not by capillarity. As diffusion of the frit constituents into the refractory is more difficult for layers formed at the interface which are thicker and richer in large ZrO_2 particles, the corrosion levels of the specimens AZS1711 were always lower.

3.2. Isostatically pressed Cr_2O_3-refractories

The isopressed Cr_2O_3-refractories were mainly constituted by coarse Cr_2O_3 grains and presented large similar values of open porosity (≈16–17%). The corrosion process in both materials led to similar microstructural modifications while the extensions of corrosion were significantly different and determined by the impurities, which were responsible for the characteristics of the matrices, and the composition of the frits.

The characteristic features of the corrosion process of these materials are summarised in Figs. 8–13. For both materials, the corrosion process led to the formation of reaction particles at the frit–refractory interfaces, identified as $ZnCr_2O_4$ by SEM-EDS. As discussed in Part I,[1] the remaining material in the post mortem specimens was larger than the starting one for both materials. This can be explained by the expansive reaction of formation of the new phase, $ZnCr_2O_4$, during the corrosion process. This phase should be more refractory than the possible $ZnAl_2O_4$ that was not detected in the AZS tested specimens.

In Figs. 8 and 9 low magnification micrographs of the interfaces between the HTF and the refractories together with EDS analyses are shown. For both materials $ZnCr_2O_4$ particles were observed close to the frit–refractory interfaces. Significant amounts of ZnO were found until depths of ≈200 μm and 500 μm for the materials containing the highest (CR-95WB) and the lowest (ZC-85) Cr_2O_3 proportions, respectively. The other constituents of the frit were found at larger depths (≈2000 μm) which were similar for both materials.

The microstructure and width of the reaction layers for both materials and frits are shown in the SEM micrographs collected in Figs. 10–13.

The reaction layers of specimens tested using the LTF were formed by independent $ZnCr_2O_4$ particles located between the coarse Cr_2O_3 grains (Figs. 10 and 12). The widths of the reaction layers were variable but always smaller than 50 μm and 100 μm for materials CR-95WB (Fig. 10) and ZC-85 (Fig. 12), respectively.

The reaction layers of specimens tested using the HTF were also constituted by $ZnCr_2O_4$ particles, but in this case they were forming a continuous phase that surrounded the Cr_2O_3 grains (Figs. 11 and 13). The widths of the reaction layers were variable at about 200 and 500 μm for materials CR-95WB (Fig. 11) and ZC-85 (Fig. 13), respectively, which coincides with the penetration depths of ZnO (Figs. 8b and 9b).

The shape and habit of the well-formed facetted $ZnCr_2O_4$ crystals (Figs. 10b and 12b) clearly indicates that they crystallized slowly from a liquid saturated in Cr and Zn. Such liquid will be formed by reaction between the frits and the constituents of the refractories. Consequently, the widths of the reaction layers formed by the interaction of the refractories with the

HTF (Figs. 11a and 13a), with higher amounts of ZnO (8.6 and 3.5 wt.% for the HTF and the LTF, respectively), were larger than those formed from the LTF (Figs. 10a and 12a). As a difference from the AZS refractories discussed above, the low viscosity and low surface tension molten frits might penetrate these refractories through their open porosity. The fact that the reaction layers formed in the ZC-85 specimens (Figs. 10a and 11a) were larger than those formed in the CR-95WB ones (Figs. 12a and 13a) for both frits cannot be explained in terms of porosity differences. Thus, compositional differences should be responsible for such behavior.

As discussed for the AZS materials, ZrO_2 presents very low solubility in silica glasses, thus, the ZrO_2 particles present in material ZC-85 would increase the corrosion resistance of this material. On the contrary, material ZC-85 had a significant amount of fluxing impurities (≈4 wt.%) that led to glass formation in the fine fraction.[1] Penetration of the frits would also take place by reaction between them and the remaining glass, thus, enhancing the extent of corrosion in this material. As a result, the reaction layers formed in the ZC-85 specimens tested using both frits (Figs. 12 and 13) were thicker than those formed in the high purity CR-95WB ones (Figs. 10 and 11).

The spinel layers formed at the interfaces frit–refractory will act as physical barriers closing porosity, thus, impeding further access of the frit constituents to the bulk of the refractory. Moreover, the composition of the frit close to the interface will lack ZnO and, consequently, it will become more viscous and its corrosive potential will be diminished. Both facts explain the excellent behavior of the Cr_2O_3-based materials in contact with molten frits.

4. Conclusions

Macroscopic analyses of corrosion test specimens have limited prediction capacity when dealing with materials such as fused cast AZS and isostatically pressed Cr_2O_3-based refractories in which extremely different corrosion mechanisms take place. In these cases, prediction requires establishing the corrosion mechanism from microstructural analyses of corroded pieces.

Corrosion of AZS refractories by frits occurs by dissolution of the crystalline constituents of the refractory, Al_2O_3 and ZrO_2, in the frit at the frit–specimen interface, and in the glass formed in the bulk of the specimens by reaction of the frit components with the glass constituent of the material. The dissolution levels of ZrO_2 and Al_2O_3 are determined by their solubility limit in SiO_2–alkali glasses.

Corrosion of Cr_2O_3-based refractories is controlled by the capillar penetration of the molten frit through the open pores. The corrosion process occurs by dissolution of Cr_2O_3 in the frit followed by the formation of a protective spinel ($ZnCr_2O_4$) layer by precipitation once the solubility limit of spinel in the resulting glass is reached. The formed spinel layer acts as a physical barrier for the penetration of the fused frit.

Acknowledgements

In memoriam to our colleague Carlos Fueyo. Authors are indebted to Mrs. M.J. Mari Juan for her collaboration in corrosion studies.

We thank Vesuvius-VGT-Dyko (Düsseldorf, Germany) and Saint Gobain (France) for kindly supplied the refractory materials used in this work. The authors acknowledge the financial support of Esmaltes S.A. and projects CDTI-01-0389 and MAT2009-14369, from Spain.

References

1. Pena P, Criado E, Bakali J, Baudín C. Dynamic corrosion of Al_2O_3–ZrO_2–SiO_2 and Cr_2O_3 – containing refractories by molten frits. Part I: macroscopic analysis. *J Eur Ceram Soc* 2011;**31**:697–703.
2. Recasens J, et al. Étude des phénomènes de diffusion à l'interface verre-réfractaire aluminesilice-zircone électrofondu. *Glastechn Ber* 1972;**45**(12):552–7.
3. Manfredo LJ, McNally RN. Solubility of refractory oxides in soda-lime glass. *J Am Ceram Soc* 1984;**67**(8):C-155–8.
4. Beerkens R, Van Dijk F, Dunk M. Reactions and interactions between tank refractory and glass melt. *Glastech Ber: Glass Sci Technol Suppl C* 2004;**77**:35–51.
5. Dunkl M, Boymanns G. Considerations to the behaviour of different refractories in glass melts regarding the formation of boundary layers. *Glass Sci Technol: Glastech Ber Suppl C2* 2000;**73**:282–3.
6. Hansson R, Zhao BJ, Hayes PC, Jak E. A reinvestigation of phase equilibria in the system Al_2O_3–SiO_2–ZnO. *Metall Mater Trans B: Process Metall Mater Process Sci* 2005;**36**(2):187–93.
7. Chartrand P, Pelton AD. *CALPHAD: Comput Coupl Phase Diagr Thermochem* 1999;**23**(2):219–30. Phase Diagrams for Ceramists. Am Ceram Soc, vol. 14, Figure 11256.
8. Kato K. System Na_2O–ZrO_2–SiO_2. *Yogyo Kyokaishi* 1982;**90**(1):1–7.
9. Zachariasen WH. The atomic arrangement in glass. *J Am Chem Soc* 1932;**54**:3841–51.
10. Dietzel AZ. Glass structure and glass properties I. *Glastech Ber* 1948;**22**(3–41):41–50.